Supplement of Atmos. Chem. Phys., 26, 11683–11693, 2026
https://doi.org/10.5194/acp-26-11683-2026-supplement


Atmospheric Chemistry and Physics Open Access

*Supplement of*

# Quantitative insights into regime-dependent aerosol pH variability in ammonia-rich urban Beijing from explainable machine learning

**Jing Duan et al.**

*Correspondence to:* Ru-Jin Huang (rujin.huang@ieecas.cn)

**S1. Sampling and instrumentation**

The field campaign was carried out at an urban site located on the rooftop of a five-story building (~20 m above ground) at the National Center for Nanoscience in Beijing (39.99°N, 116.32°E). The site is situated near the 4th Ring Road and is influenced by mixed residential, commercial, and traffic emissions (Duan et al., 2020; Gu et al., 2020). Continuous measurements were performed from 21 December 2014 to 31 December 2015.

Non-refractory $PM_1$ (NR-$PM_1$) species, including organics (OA), sulfate ($SO_4^{2-}$), nitrate ($NO_3^-$), ammonium ($NH_4^+$), and chloride ($Cl^-$), were quantified using an Aerodyne quadrupole aerosol chemical speciation monitor (Q-ACSM) with a time resolution of ~30 min (Ng et al., 2011). Ambient aerosols were sampled through a 3/8 in. stainless-steel tube at a flow rate of ~ 3 L $min^{-1}$, and the coarse particles were removed by an University Research Glassware (URG) cyclone (model: URG2000-30ED) with a 2.5 μm cut in front of the sampling inlet. Before entering the ACSM, particles were dried using a Nafion dryer (MD110-48S; Perma Pure, Inc., Lakewood, NJ, USA). The dried submicron aerosol was then subsampled into the ACSM at 85 cc $min^{-1}$, controlled by a 100 μm critical orifice. Within the ACSM, particles were focused into a narrow beam by an aerodynamic lens and vaporized on a heated surface (~600 °C). The resulting vapor was ionized with electron impact and chemically characterized with a quadrupole mass spectrometer. Instrument calibration was carried out using monodisperse 300 nm ammonium nitrate particles generated by an atomizer (Model 9302, TSI Inc., Shoreview, MN, USA) and size-selected by a differential mobility analyzer (DMA; TSI Model 3080) to determine the response factor (RF) and ionization efficiency (IE) (Ng et al., 2011).

Ambient ammonia ($NH_3$) concentrations were measured using a Picarro G2103 analyzer (Picarro Inc., USA), which employs wavelength-scanning optical cavity ring down spectroscopy (WS-CRDS). This technique is capable of measuring $NH_3$ with a parts-per-trillion (ppt) sensitivity based on a sophisticated time-based measurement system (Maasikmets et al., 2015). The G2103 is equipped with high-precision temperature and pressure control systems to ensure the highest accuracy and lowest drift. In addition, the G2103 offers a large dynamic range, providing linear response into the parts-per-million (ppm) range without dilution,

concentration and sample preparation.

Meteorological parameters, including temperature and relative humidity (RH), were simultaneously recorded by an automatic weather station (MAWS201, Vaisala, Vantaa, Finland).

**S2. Calculation of excess NHx**

Excess NHx in this study represents the portion of total NHx (gas-phase $NH_3$ plus particle-phase $NH_4^+$) that remains after neutralizing the major inorganic acidic species ($SO_4^{2-}$, $NO_3^-$, and $Cl^-$) in the aerosol (i.e., the required NHx) (Liu et al., 2017).

Thus, excess NHx is defined as:

Excess NHx = Total NHx- Requid NHx

Where

$$\text{Total NHx} = 17 \times \left(\frac{[NH_3]}{17} + \frac{[NH_4^+]}{18}\right) \quad \text{(S1)}$$

$$\text{Required NHx} = 17 \times \left(\frac{[SO_4^{2-}]}{48} + \frac{[NO_3^-]}{62} + \frac{[Cl^-]}{35.5}\right) \quad \text{(S2)}$$

$[NH_3]$, $[NH_4^+]$, $[SO_4^{2-}]$, $[NO_3^-]$, and $[Cl^-]$ are the measured mass concentrations (μg $m^{-3}$). A positive excess NHx (μg $m^{-3}$) indicates ammonia-rich conditions, whereas a negative value denotes ammonia-poor conditions (Song et al., 2018).

**Table S1.** Monthly performance metrics ($R^2$, RMSE, MAE) of the XGBoost model from leave-one-month-out cross-validation.

| Month | $R^2$ | RMSE | MAE |
|---|---|---|---|
| Dec-14 | 0.64 | 0.23 | 0.15 |
| Jan-15 | 0.63 | 0.19 | 0.16 |
| Feb-15 | 0.68 | 0.23 | 0.17 |
| Mar-15 | 0.90 | 0.21 | 0.15 |
| Apr-15 | 0.94 | 0.17 | 0.12 |
| May-15 | 0.97 | 0.13 | 0.08 |
| Jun-15 | 0.98 | 0.10 | 0.07 |
| Jul-15 | 0.97 | 0.10 | 0.06 |
| Aug-15 | 0.96 | 0.13 | 0.10 |
| Sep-15 | 0.94 | 0.19 | 0.11 |
| Oct-15 | 0.88 | 0.19 | 0.12 |
| Nov-15 | 0.90 | 0.11 | 0.08 |
| Dec-15 | 0.74 | 0.19 | 0.15 |
| **Average** | **0.86±0.13** | **0.17±0.05** | **0.12±0.04** |

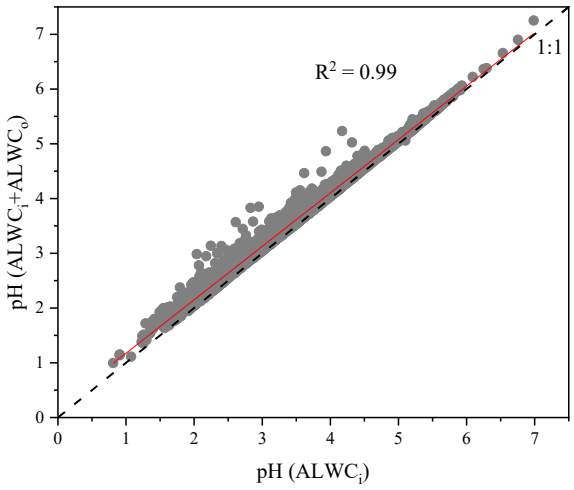


**Figure S1.** Comparison of pH calculated with and without organic aerosol water ($ALWC_o$).

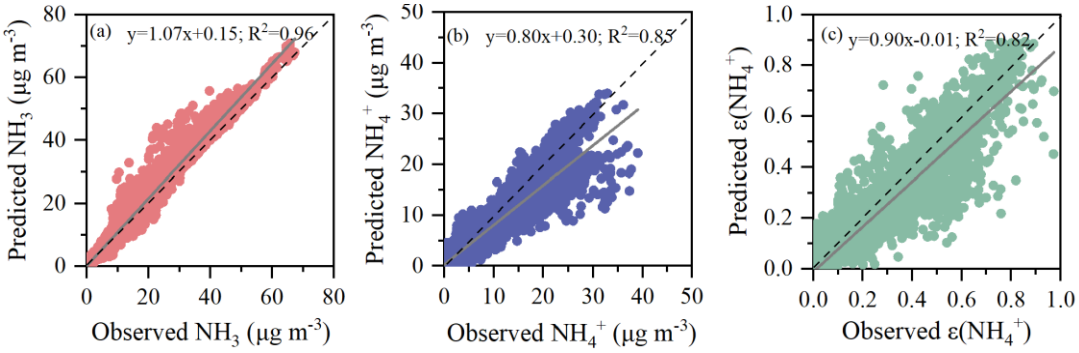


**Figure S2.** Comparisons between predicted and observed values for $NH_3$ (a), $NH_4^+$ (b), and $\varepsilon(NH_4^+)$ (c). $\varepsilon(NH_4^+)$ is calculated as the molar ratio of $NH_4^+/(NH_4^+ + NH_3)$.

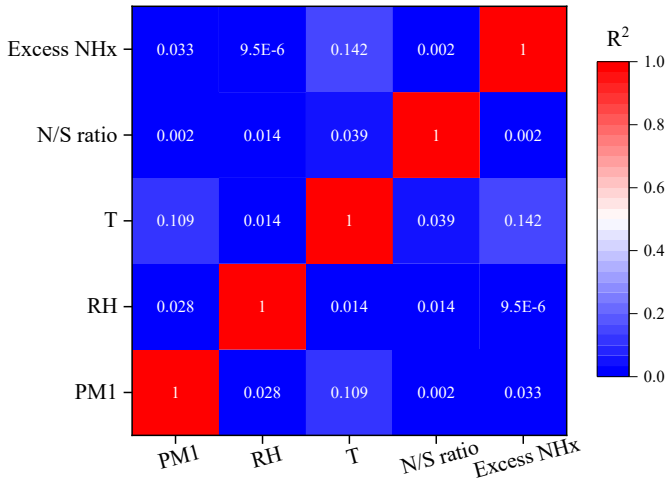


**Figure S3.** Correlation matrix of input features. The color scale represents the correlation coefficient ($R^2$).

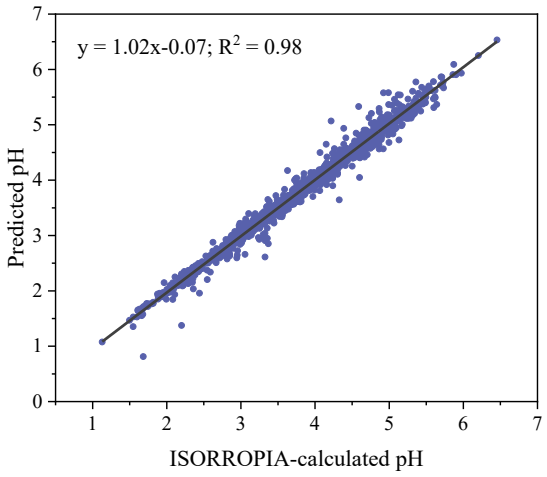


**Figure S4.** Correlation between aerosol pH predicted by XGBoost model and pH calculated using ISORRPOIA II.

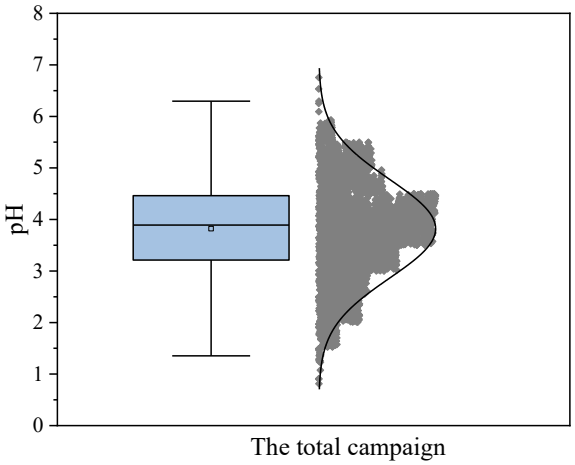


**Figure S5.** Distribution of aerosol pH in this study. The box spans the 25th–75th percentiles, with whiskers extending to the 10th and 90th percentiles. The line and square inside the box indicate the median and mean, respectively.

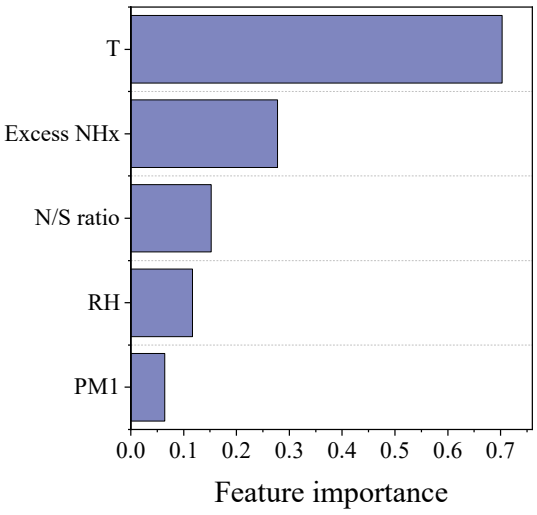


**Figure S6.** Feature importance for aerosol pH over the entire sampling period based on mean absolute SHAP values.

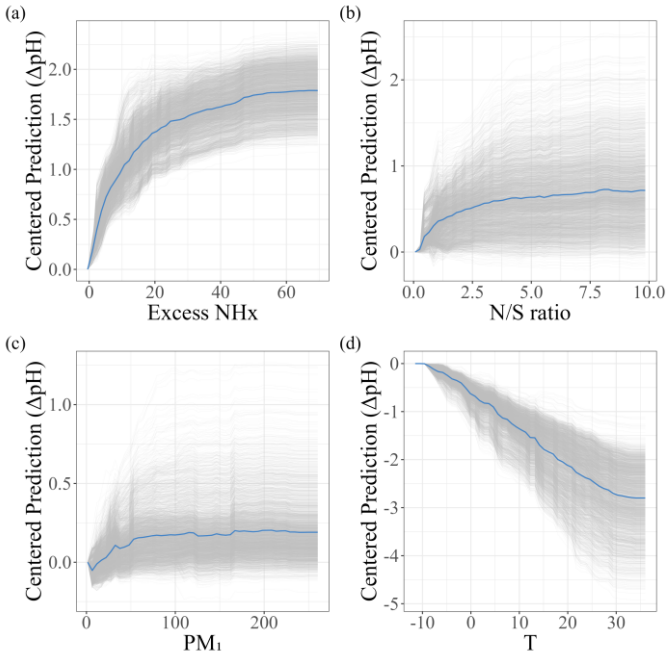


**Figure S7.** c-ICE curves of (a) Excess NHx (μg $m^{-3}$), (b) N/S ratio, (c) $PM_1$ mass loading (μg $m^{-3}$), and (d) temperature (T, ℃). Gray lines represent sample-specific effects on aerosol pH, and the blue line shows the averaged response.

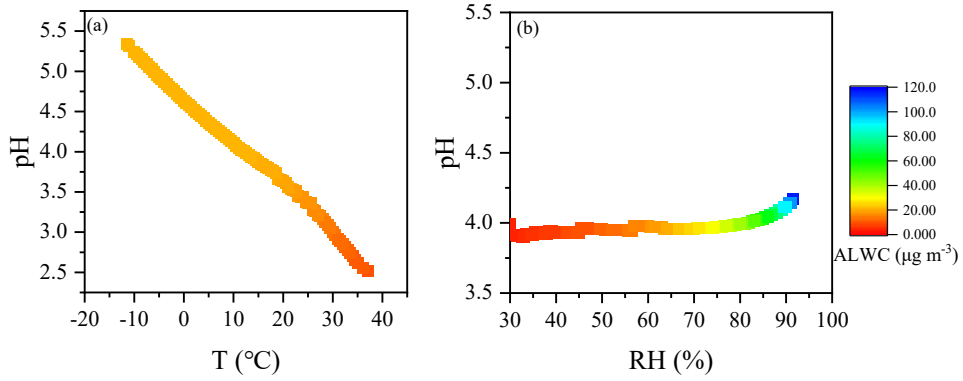


**Figure S8.** ISORROPIA II sensitivity tests of pH to temperature (a) and RH (b). In this analysis, the real-time measured values of the tested variable, while the average values of the other species were applied as the input into ISORROPIA II.

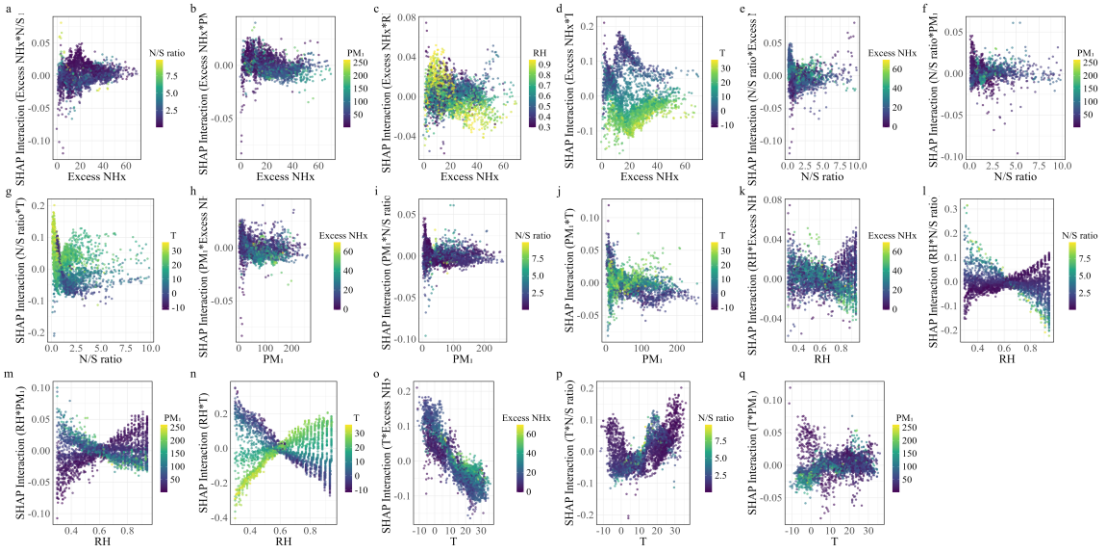

**Figure S9.** Summary plots of the SHAP interaction matrix values for pH among each pair of variables, excluding RH vs T, RH vs N/S ratio, and RH vs $PM_1$ mass, which are discussed in detail in the manuscript.

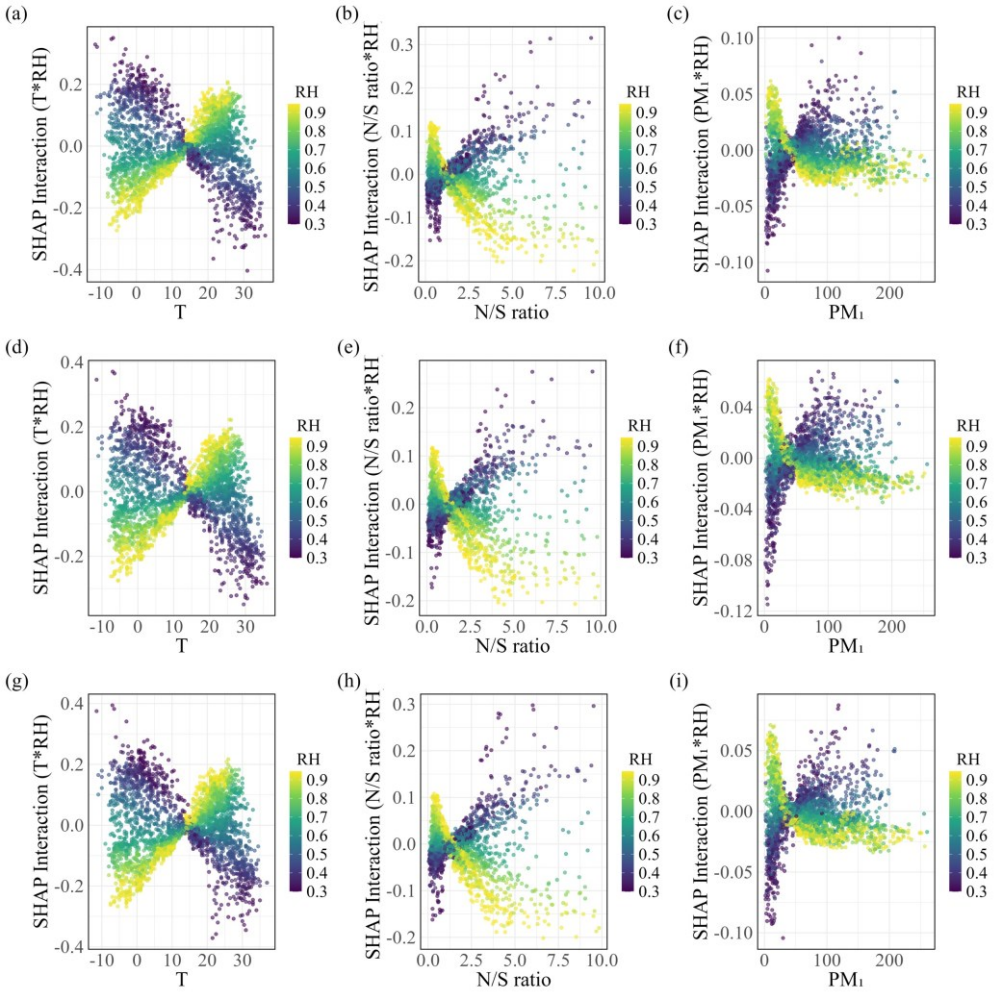


**Figure S10.** SHAP interaction plots for RH versus temperature (T, ℃), N/S ratio, and $PM_1$ mass loading (μg $m^{-3}$) under different random seeds of 1234 (a, b, c), 5678 (d, e, f), and 9012 (g, h, i). The color scale represents RH, and the SHAP interaction values indicate the direction and magnitude of the interactive contributions to pH across different regimes.

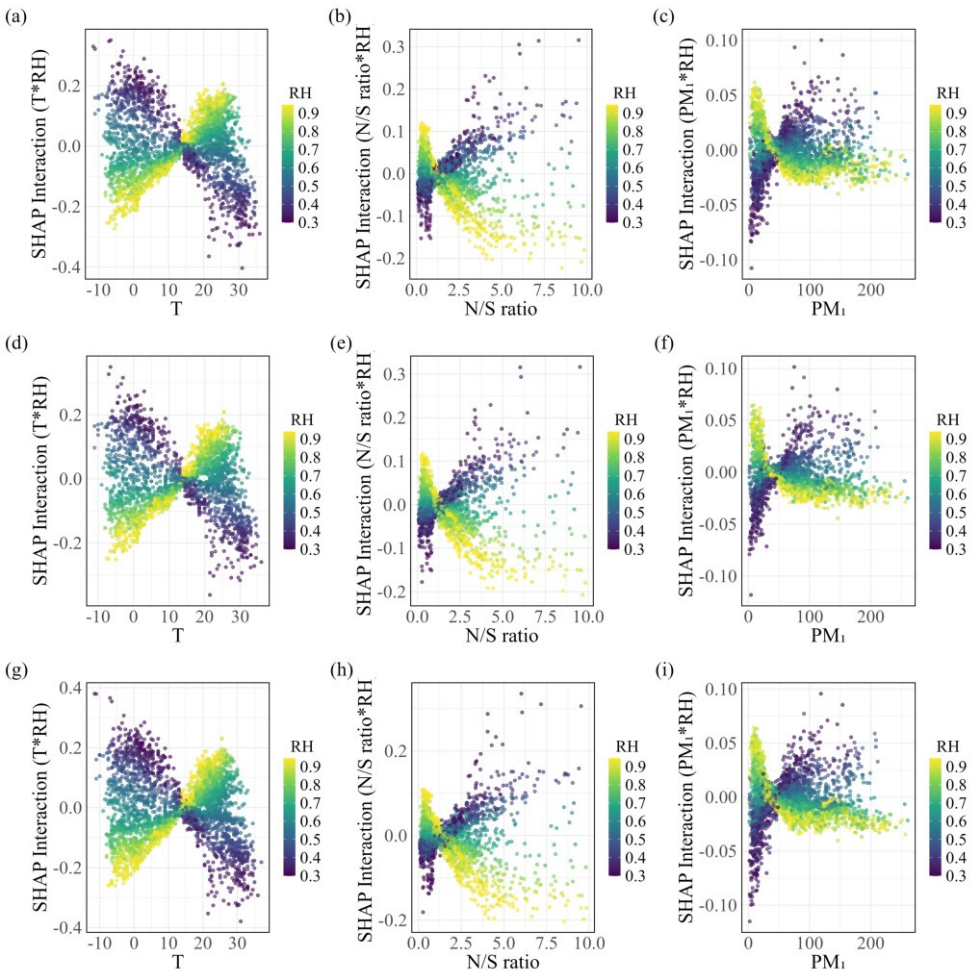


**Figure S11.** SHAP interaction plots for RH versus temperature (T, °C), N/S ratio, and $PM_1$ mass loading (μg $m^{-3}$) under different train/test split ratio of 0.7 (a, b, c), 0.6 (d, e, f), and 0.8 (g, h, i). The color scale represents RH, and the SHAP interaction values indicate the direction and magnitude of the interactive contributions to pH across different regimes.

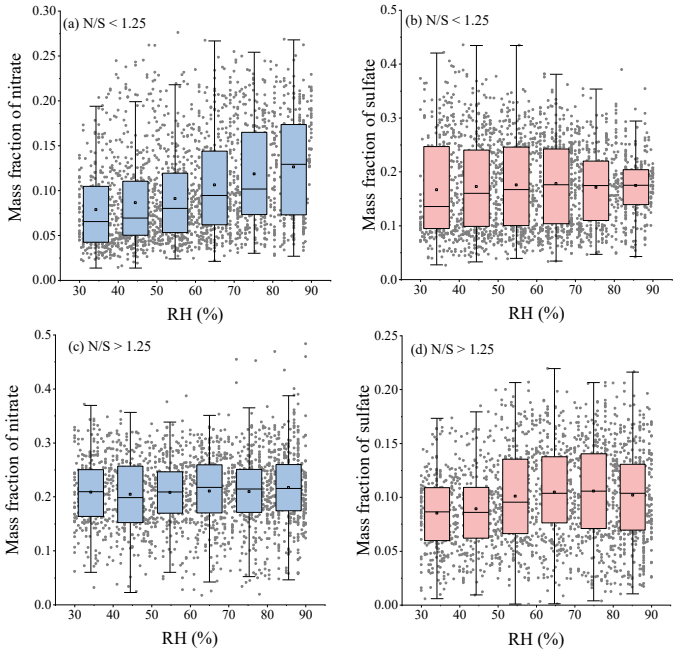


**Figure S12.** The variations in nitrate and sulfate mass fractions with RH under sulfate-dominant conditions (N/S < 1.25) (a, b) and nitrate-dominant conditions (N/S > 1.25) (c, d), respectively. The whiskers, floating boxes, lines, and squares inside the boxes denote the 10th and 90th distributions, 25th-75th ranges, median values, and mean values, respectively.

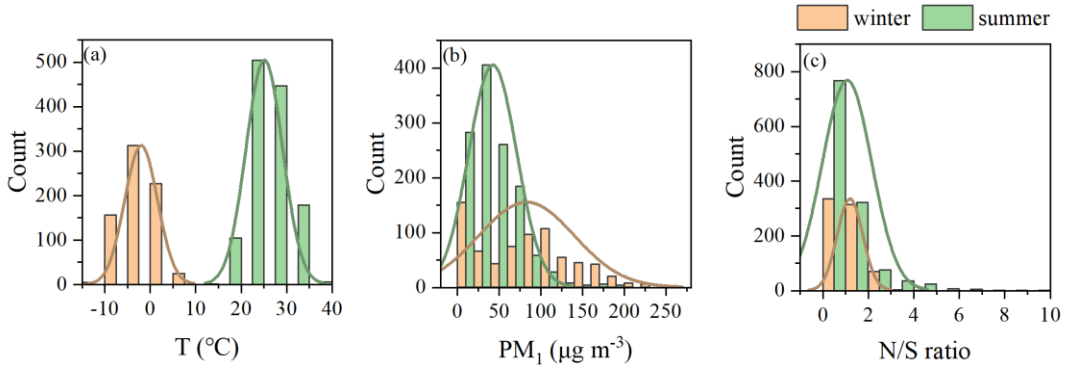


**Figure S13.** The distribution of temperature (a), $PM_1$ mass loading (b), and nitrate-to-sulfate (N/S) mass ratio (c) between summer and winter periods.

**Reference**

Duan, J., Huang, R.-J., Li, Y., Chen, Q., Zheng, Y., Chen, Y., Lin, C., Ni, H., Wang, M., Ovadnevaite, J., Ceburnis, D., Chen, C., Worsnop, D. R., Hoffmann, T., O'Dowd, C., and Cao, J.: Summertime and wintertime atmospheric processes of secondary aerosol in Beijing, Atmos. Chem. Phys., 20, 3793-3807, 10.5194/acp-20-3793-2020, 2020.

Gu, Y., Huang, R. J., Li, Y., Duan, J., Chen, Q., Hu, W., Zheng, Y., Lin, C., Ni, H., Dai, W., Cao, J., Liu, Q., Chen, Y., Chen, C., Ovadnevaite, J., Ceburnis, D., and O'Dowd, C.: Chemical nature and sources of fine particles in urban Beijing: Seasonality and formation mechanisms, Environ. Int., 140, 105732, 10.1016/j.envint.2020.105732, 2020.

Liu, M., Song, Y., Zhou, T., Xu, Z., Yan, C., Zheng, M., Wu, Z., Hu, M., Wu, Y., and Zhu, T.: Fine particle pH during severe haze episodes in northern China, Geophys. Res. Lett., 44, 5213-5221, 10.1002/2017gl073210, 2017.

Maasikmets, M., Teinemaa, E., Kaasik, A., and Kimmel, V.: Measurement and analysis of ammonia, hydrogen sulphide and odour emissions from the cattle farming in Estonia, Biosyst. Eng., 139, 48-59, 10.1016/j.biosystemseng.2015.08.002, 2015.

Ng, N. L., Herndon, S. C., Trimborn, A., Canagaratna, M. R., Croteau, P. L., Onasch, T. B., Sueper, D., Worsnop, D. R., Zhang, Q., Sun, Y. L., and Jayne, J. T.: An Aerosol Chemical Speciation Monitor (ACSM) for Routine Monitoring of the Composition and Mass Concentrations of Ambient Aerosol, Aerosol. Sci. Tech., 45, 780-794, 10.1080/02786826.2011.560211, 2011.

Song, S., Gao, M., Xu, W., Shao, J., Shi, G., Wang, S., Wang, Y., Sun, Y., and McElroy, M. B.: Fine-particle pH for Beijing winter haze as inferred from different thermodynamic equilibrium models, Atmos. Chem. Phys., 18, 7423-7438, 10.5194/acp-18-7423-2018, 2018.